DFT Study on Ferroelectricity of $BaTiO_3$

Zhao-Xu Chen, Yi Chen, and Yuan-Sheng Jiang*

Lab of Mesostructured Materials Chemistry and Department of Chemistry, Nanjing University, Nanjing 210093, People's Republic of China

Received: September 13, 2000; In Final Form: March 23, 2001

The ferroelectricity of $BaTiO_3$ is investigated with the plane-wave pseudopotential method and the LCAO quantum chemical approach in the framework of density functional theory (DFT). Potential energy surfaces of various atomic displacements and the influence of lattice strain and lattice volume on the surfaces are examined. On the basis of the potential surfaces, phonon frequencies are also computed, which are in agreement with experiment results. The obtained potential energy surfaces show that the ferroelectric phase transition (from the cubic to the tetragonal phase) is decisively controlled by Ti displacement. The larger the lattice volume and the ratio c/a, the deeper the potential well. The calculated electronic populations and static charges show that from cubic to tetragonal phases Ti and O1 lose charges whereas Ba and O2 gain charges. The bond orders reveal that Ba−O has some extent of covalency, and during the phase transition the chemical bonding between metal and oxygen atoms, especially the Ti−O1 bond, is enhanced. Our results seem consistent with the vibronic theory about the origin of ferroelectricity of $BaTiO_3$.

1. Introduction

Ferroelectric materials are characterized by having a polarization direction that can be switched in response to an external electric field, which generates many technical applications. Ferroelectric perovskites have been the most important type of ferroelectrics for both theoretical and practical purposes.[1] These compounds have a chemical formula ABO_3, where A is a monovalent or divalent metal cation and B is a penta- or tetravalent transition metal atom. The perfect perovskite belongs to a cubic lattice of which the unit cell structure is shown in Figure 1. This cubic lattice (paraelectric phase) often distorts to the ferroelectric phase of lower symmetry at decreased temperatures. For barium titanate ($BaTiO_3$), a typical (2:4:2 type) perovskite ferroelectric, such a transformation takes place at 130 °C. As the temperature is lowered, two additional phase transitions occur. In company with the phase transition, atomic displacements take place and the macroscopic strain appears along the ferroelectric direction.

Recently, first-principles calculations have been performed to study the electronic structures of perovskite compounds for gaining an insight into the nature of ferroelectricity. Local density approximation (LDA) investigations show that the ferroelectric instability is sensitive to lattice volume.[2−6] On the basis of full-potential linear augmented plane-wave (FLAPW) calculations, Cohen and Krakauer suggest that the ferroelectricity originates from the delicate balance between the long-range Coulomb force which favors the ferroelectric phase and the short-range repulsion which favors the paraelectric phase.[2−4] To investigate the Coulomb interactions, some researchers have computed the Born dynamic charges (Z^*) for a series of perovskites.[7−9] It is found that the anomalously large Z^* is a general feature of perovskites. Electronic structure calculations show that Ti−O hybridization plays an important role in ferroelectric phase transition.[2−4,10−14] The LDA calculated phonon frequencies[2,9,15−16] at Γ point at experimental volume of cubic $BaTiO_3$ agree with the observed results and consistently show that there is an unstable mode due to one imaginary frequency. King-Smith and Vanderbilt performed accurate first-principles pseudopotential calculations on eight ABO_3 perovskites. Their LDA calculations correctly predicted the symmetry of the ground-state structures of the some compounds. They found that zone-center instabilities in the cubic perovskite structure were very common. Zhong and Vanderbilt demonstrated that the antiferrodistortive instabilities were almost as common as ferroelectric ones in cubic perovskite compounds.[18] Even more encouraging is that their obtained sequence of transition and spontaneous polarization of $BaTiO_3$ are in good agreement with the experiment.[19]

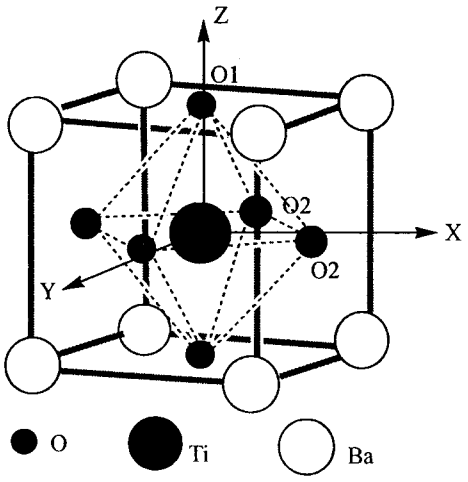

Figure 1. Illustration of atomic positions and cubic phase structure of $BaTiO_3$.

Although many achievements have been realized, some problems are still unsettled. For example, there are two theoretical points of view about the origin of ferroelectricity of ABO_3 perovskites. Besides Cohen's theory, the vibronic theory suggests that the ferroelectric instability stems from the occur-

* Corresponding author.

10.1021/jp0032558 CCC: $20.00
Published on Web 05/26/2001

rence of new covalency by distortion.[20] The long-range force can only soften the lattice without producing ferroelectric instability. The direction of charge transfer during the ferroelectric phase transition is also questionable. Xu et al. point out that slight charges may transfer from Ba to O in the tetragonal phase as the result of relative position shift and the small volume effect.[12] Weyrich and Madenach[21,22] think that the additional covalency produced by the lower symmetry gives rise to a charge transfer from oxygen to titanium. Meanwhile, Nelson[23] emphasized that charge transfer from O to Ti would not favor the ferroelectricity. It has been pointed out[2−4] that the covalency of the B−O bond plays a key role in producing the ferroelectricity of perovskites. However, previous investigations are generally confined to qualitative results, with little information about covalency strength of bonds in different structures of $BaTiO_3$. Thus quantitative results are expected to elucidate the nature of ferroelectricity from chemical bonding theory.

Another issue with which we are concerned in this paper is the potential energy surfaces, because they are important in molecular dynamic simulation and in elucidating the nature of ferroelectricity. Cohen and Krakauer have investigated the potential energy surface of atomic displacements in $BaTiO_3$ (and $PbTiO_3$) within the experimental soft mode along [001] and [111] directions by means of FLAPW calculations[2−5] in LDA framework. They found that the results were quite sensitive to lattice volume, and typical LDA errors in volume could lead to significant errors in the potential surface for ferroelectric distortions.[4] It is known that GGA (generalized gradient approximation)[24] is an improvement over LDA. Recently Singh has performed a comparative study on $BaTiO_3$ and $KNbO_3$ using the general potential LAPW (linear augmented plane-wave) method at both LDA and GGA levels.[25] It is shown that for $KNbO_3$ GGA yields an equilibrium volume that is much closer to the experimental value than LDA. However, for $BaTiO_3$, GGA overestimates the equilibrium volume and the deviation is nearly as large as that of LDA with opposite sign. The author attributed the error to an incorrect description of the ions. Very recently Tinte and co-workers[16] have studied several perovskites with GGA proposed by PBE (Perdew−Bueke−Ernzerhof). It is found that by adjusting the parameter κ, GGA can yield equilibrium volume in good agreement with experiments. Our calculation will show that GGA can produce satisfactory lattice parameters of $BaTiO_3$ with the Kerker pseudopotentials.

With all of the above in mind, in the present paper we report the investigations of the potential energy surfaces of atomic displacements and examine their dependence on the lattice volume and lattice strain with the pseudopotential approach[26] in GGA framework. We also performed LCAO calculations to explore the chemical bonding and charge distribution of the perfect and distorted $BaTiO_3$.

The organization of this paper is as follows: In section 2 the methodology is presented. In section 3 potential energy surfaces of various atomic displacements and the effects of lattice volume and lattice strain are discussed. The net atomic charge, electronic population and bond order of $BaTiO_3$ in the different structures are also presented and analyzed in section 3. Finally concluding remarks are given.

2. Methodology

2.1. Potential Energy Surface. In this paper, potential energy surface calculations are performed with the CASTEP (Cambridge Series of Total Energy Program) code,[27] implemented in the Cerius2_3.5 Version of Molecular Simulations Inc. as an application program. This code employs a plane-waves basis set for the valence electrons where atomic cores incorporate via separable pseudopotentials.

TABLE 1: Reference Configuration and Core Radii of the Pseudopotentials

	Ba[a]	Ti	O
configuration	$5s^25p^{5.75}5d^{0.25}$	$3d^24s^2$(s,d) $3d^24s^{0.75}4p^{0.25}$(p)	$2s^22p^4$(s,p) $2s^12p^{1.75}3d^{0.25}$(d)
radii (a.u) (s,p,d)	2.7	2.5	1.8

[a] Relativistic effect included.

In pseudopotential scheme, the total energy is expressed as follows:[26,28]

$$E_{tot} = E_{kin} + E_{e-c} + E_{xc} + E_{HF} + E_{ewald} \quad (1)$$

where E_{kin} is the kinetic energy of electrons, E_{e-c}, E_{xc}, E_{HF}, and E_{ewald} represent electron−core, exchange-correlation, electron−electron, and (lattice) core−core interaction energies respectively. The electron−core interaction energy can be further split into the sum of local potential energy and nonlocal potential energy. Thus one has

$$E_{tot} = E_{kin} + E_{loc} + E_{non} + E_{xc} + E_{HF} + E_{ewald} \quad (2)$$

All calculations are performed in density functional theory (DFT) framework.[29−30] The exchange-correlation energy in the GGA scheme adopts the Perdew−Wang functional.[24,31] Integration over the Brillouin zone is replaced by sums on a mesh of special **k**-points ($4 \times 4 \times 4$).[32−33] A kinetic cutoff of 850 eV, corresponding to about 3600 plane-waves, is used throughout our work. The semilocal norm-conserving pseudopotentials for Ba, Ti, and O were generated using the optimized version of Kerker's scheme[34] and transformed into the separable form of Kleinman−Bylander pseudopotentials.[35] The 5s, 5p, and 6s levels of barium, the 3d and 4s levels of titanium, and the 2s and 2p levels of oxygen are treated as valence states. Table 1 lists the reference configuration and core radii of the pseudopotentials used in this paper.

The default convergence criteria in the program are adopted in the calculations. Under the above calculation conditions, the calculated dielectric constant of the cubic phase (using the scissor operators technique with a scissor shift of 1.04 eV) is 5.74 (the experimental value is 5.40[36]). The optimized lattice constant (3.990 Å) of the cubic $BaTiO_3$ is quite close to the experimental result (3.996 Å).[37] As pointed out in the Introduction, Singh[25] found that GGA overestimated the equilibrium volume of $BaTiO_3$. The error was nearly as large as that given by LDA with the opposite sign. We have also optimized the equilibrium volume of $BaTiO_3$ with Troullier−Martins pseudopotetials[38] at GGA and LDA levels, respectively. The obtained lattice parameters are 4.17 Å (GGA) and 4.18 Å (LDA), respectively. The above results seem to indicate that the good agreement between our optimized lattice parameter and the experimental one is due to the pseudopotentials we have adopted, of which the error happens to roughly offset the GGA's.

The potential energy surfaces of atomic displacement are calculated along the experimental soft mode without lattice strain ($c/a = 1$). The effect of lattice volume on the potential energy surface is examined by scanning the potential energy surface of Ti atomic displacement with respect to the lattice constant in the absence of lattice strain. To look into the influence of lattice strain on the potential surface, we have also calculated

TABLE 2: Lattice Constant and Atom Positions of the Unit Cell for Perfect and Distorted $BaTiO_3$[a]

structure	lattice constant (Å)	Ba	Ti	O1	O2
Cubic	$c = 4.010$	(0, 0, 0)	(0.5, 0.5, 0.5)	(0.5, 0.5, 0.0)	(0.5, 0. 0, 0.5)
$Tetr_{Ti}$	$a = b = c = 4.010$	(0, 0, 0)	(0.5, 0.5, 0.526)	(0.5, 0.5, 0.0)	(0.5, 0.0, 0.5)
$Tetr_{Tio12}$	$a = b = c = 4.010$	(0, 0, 0)	(0.5, 0.5, 0.520)	(0.5, 0.5, −0.0250)	(0.5, 0.0, 0.4870)
$Tetr_{exp}$	$c = 4.0413$, $a = b = 3.997$	(0, 0, 0)	(0.5, 0.5, 0.5203)	(0.5, 0.5, −0.0258)	(0.5, 0.0, 0.4877)

[a] $Tetr_{exp}$ refers to the experimental tetragonal structure at 280 K.[47]

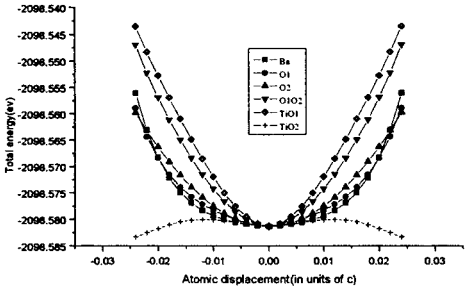

Figure 2. Potential energy curves of various displacements.

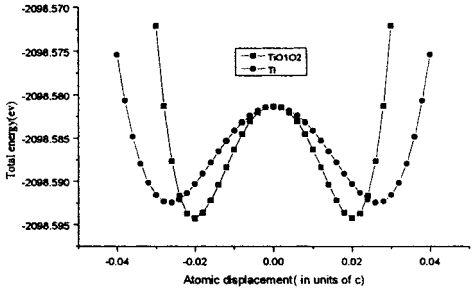

Figure 3. Potential energy curves of atomic displacements.

the hypersurface for Ti displacements at constant lattice volume with different ratio of c/a.

2.2. Electronic Structure Calculations. We employ DSolid, the new version of the DMol program,[39−40] to study the electronic structures of $BaTiO_3$ solids. The DMol code has witnessed wide application in biochemistry, environmental science, and materials science.[41−44] The DSolid code used for periodic systems works on an equal footing with the same atomic bases and number of mesh points. The fine grid and standard DMol partitioning schemes were employed, which amounts to about 2000 integration points per atom. After a series of tests and comparisons on various DFT calculations, we choose the BLYP[45,46] gradient correction as the correlation-exchange term. Calculations including relativistic effects (using double numerical polarization basis sets for O and Ti and the minimal numerical basis set for Ba)[39,40] produce more reasonable results.

Four kinds of structure have been studied in this paper. Two of them are the cubic (Cubic) and experimental tetragonal structures ($Tetr_{exp}$), respectively. The other two (denoted as $Tetr_{Ti}$ and $Tetr_{TiO12}$ respectively) correspond to the local minima of potential energy of Ti displacement alone and the coupled displacement of Ti and O atoms along the [001] direction (i.e., the Z axis in Figure 1), respectively. Table 2 lists the lattice parameters and atom positions for the four types of structure. All calculations were carried out on an SGI workstation in our department.

3. Results and Discussions

3.1. Potential Energy Surfaces of Atomic Displacement. The potential energy curves for various atomic displacements and coupled atomic displacements along the [001] direction without tetragonal strain ($c/a = 1$, $c = 4.01$ Å) are shown in Figure 2 and Figure 3. In Figure 2, the solid squares (■) represent the potential energy curve referring to Ba displacement alone. Solid rhombus (◆) specify the potential energy surface of coupled displacement of Ti and O1 in the ratio consistent with experiments. The rest of the curves can be handled in a similar way. From Figure 2 one can see that the displacements of Ba, O1, and O2 uniquely produce a single well in the potential energy curve. The potential wells induced by the coupled displacements of Ti and O1 and of O1 and O2 are also single wells. The single well for the coupled displacements of Ti and O2 looks flat and wide, different from others.

TABLE 3: Frequencies (cm^{-1}) of the Γ_{15} Modes

	LDA[a]	LDA[b]	LDA[c]	LDA[d]	GGA[b]	GGA[e]	expt[f]
TO1	72*i*	239*i*	219*i*	178*i*	205*i*	112*i*	soft
TO2	161	163	166	177	167	184	182
TO3	397	454	453	468	461	468	482

[a] Reference 2. [b] Reference 16. [c] Reference 15. [d] Reference 9. [e] Present work. [f] Reference 48.

Figure 3 displays the double wells in the potential energy curve of Ti displacement and that of coupled displacements of Ti, O1, and O2. These two curves look similar with double minima equally apart from the origin (the cubic structure). Minima locate at $\pm 0.026c$ (c refers to the lattice constant) and $\pm 0.020c$ with stabilization energies equal to 11.1 meV and 12.9 meV, respectively. It is noted that our GGA calculated well depth (12.9 meV) is shallower than the LDA result [25.6 meV at (6,6,6) mesh].[6] We have also calculated the potential energy surface for the combined displacement of Ti and O atoms at LDA level. The obtained well depth(∼10 meV) is also lower than that of ref 6, indicating that the discrepancy between our GGA result and the previous LDA calculation is mainly due to other factors. One possible factor is the quality of Brillounin zone (BZ) integration.[6,17] As pointed out in ref 6, the well depth decreased by ∼8 meV on reducing the quality of the BZ integral from a (6,6,6) to a (4,4,4) Monkhorst Pack mesh. Another factor might be the different pseudopotentials adopted. We note that in ref 6 the semicore states of titanium are handled as valence states, and in barium pseudopotential relativistic effects are not included.

Following the guideline of ref 2, we have calculated the frequencies of the Γ_{15} modes of $BaTiO_3$ based on the potential energy surfaces given in this paper. Results are displayed in Table 3, together with the results from other research groups. Our calculated values for TO2 (184 cm^{-1}) and TO3 (468 cm^{-1}) agree well with available experimental and theoretical values. TO1 is imaginary, corresponding to the experimentally observed soft mode. For this mode, the difference between the theoretical results is relatively large. Our value (112*i*) is moderate.

The above results reveal that either the displacement of Ti alone or the coupled manner of Ti and O favors the transformation from the cubic phase to the tetragonal phase. Unlike $PbTiO_3$ where the phase transition is mainly controlled by the displacement of Pb,[49] Ti displacement is the dominant factor for the ferroelectricity of $BaTiO_3$. Recently, Ghosez and co-workers[50]

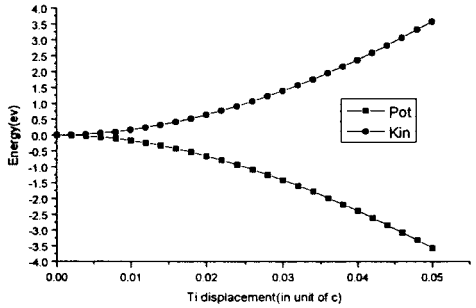

Figure 4. Variation of kinetic energy and potential energy with Ti displacement.

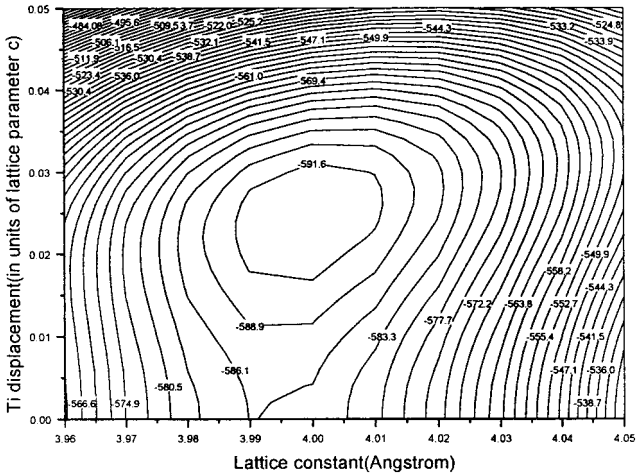

Figure 5. Potential energy surface of Ti displacement at different lattice volume (energy in units of meV).

have performed a lattice dynamic study on $BaTiO_3$, $PbTiO_3$, and $PbZrO_3$. Their investigations show that the unstable eigenvector of $BaTiO_3$ is dominated by Ti displacement along Ti−O−Ti chain. In other words, Ti displacements play a decisive role in the ferroelectric instability of $BaTiO_3$, which is in agreement with our result. This may also indicate the validity of the picture proposed early by Slater[51] that the ferroelectricity of $BaTiO_3$ originates from the rattling of Ti in the cage of oxygen.

The variation of kinetic energy (E_{kin}) and potential energy (E_{pot} where $E_{pot} = E_{loc} + E_{non} + E_{HF} + E_{EX} + E_{ewald}$) shows relationship to chemical bonding.[28] To make a deeper understanding of the ferroelectric phase transition, in Figure 4 we have depicted the plots of E_{kin} and E_{pot} with respect to Ti-atom displacement. It is notable from the figure that the potential energy (E_{pot}) decreases with Ti displacement, whereas the kinetic energy (E_{kin}) increases. As Ti shifts toward O1, the distance between Ti and O1 shortens and the localized chemical bond is enforced, giving an increase in kinetic energy and decrease in potential energy. This result seems to imply that distortion results in the formation of new covalency, which is consistent with LCAO calculations (see later section).

3.2. Lattice Volume and Lattice Strain. Investigations[2−4,6,25] show that the potential energy surface is sensitive to the lattice volume. The lattice strain also has significant effect on the depth of the potential well.[2−4] As the potential energy surface of Ti displacement alone is very similar to that of the coupled displacement of Ti and O atoms, here we examine only the effect of lattice volume and lattice strain on the potential energy surfaces of Ti displacement. The calculated hypersurfaces are displayed in Figure 5 and Figure 6, respectively. In Figure 5, the potential energy hypersurface is plotted in terms of Ti atomic displacement, and the lattice volume is specified by lattice

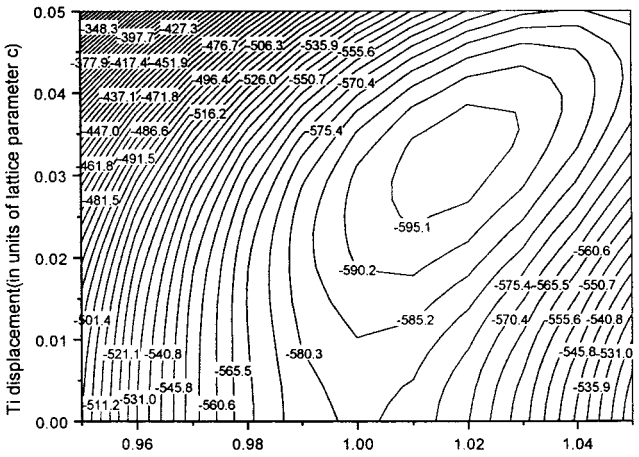

Figure 6. Hypersurface of coupling of lattice strain and atomic displacement at constant volume (energy in units of meV).

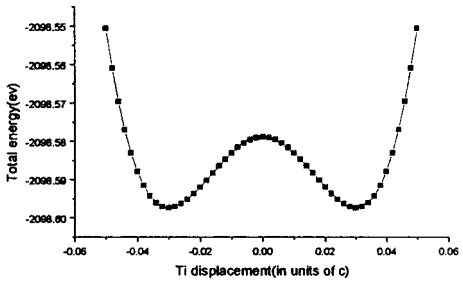

Figure 7. Potential energy curve of Ti displacement at the experimental tetragonal structure.

constant. Figure 6 is similar to Figure 5 where in plotting the hypersurface, the lattice volume is replaced by the lattice strain (c/a). From Figure 5 one easily inspects that the depth of the potential well varies in proportion to the lattice volume. The larger the volume, the deeper the well. For example, the well depth is 2.11 meV at the volume 62.10 Å^3 (lattice parameter = 3.96 Å) while it reaches 22.98 meV at 66.43 Å^3 (lattice constant = 4.05 Å). As a limit, when the lattice constant is close to or less than 3.95 Å (i.e., lattice volume = 61.63 Å^3), the potential well disappears. It is worth pointing out that LDA also predicts the vanishing energy well at ∼3.95 Å. This is consistent with the loss of ferroelectricity in titanates at high pressures.[52] The structures of $CaTiO_3$ and $SrTiO_3$ are similar to $BaTiO_3$. However, they do not exhibit ferroelectricity.[53] One possible reason might be their relatively small lattice volumes (the lattice constant is 3.89 Å for cubic $CaTiO_3$ and 3.905 Å for $SrTiO_3$).

Now we turn to analyze the effect of tetragonal lattice strain on potential surface. The lattice strain can be specified by the ratio of lattice constants, c/a, when the cubic lattice is distorted to a tetragonal one. Experiments show that the lattice strain in tetragonal $BaTiO_3$ lattice is about 1%. Contour maps displayed in Figure 6 do show the dependence of the potential energy surface of Ti displacement on the lattice strain. The trend is similar to that of lattice volume mentioned above. For instance, an increment of 50.8 meV is obtained for the potential well depth at $c/a = 1.05$ in comparison to that at $c/a = 1$. When the ratio c/a is less than 0.98, the well will disappear, which might be due to shortened distance between Ti and O1. From Figure 6 one also finds the minimum of the potential energy surface locates at $c/a = 1.01$ which is in agreement with the experimental value of c/a for the tetragonal phase of $BaTiO_3$.

To completely understand the effect of lattice strain on the potential well, we have calculated the potential energy curve (see Figure 7) of Ti displacement alone at the experimental

TABLE 4: BLYP Calculated Atomic Charges of Four Structures of BaTiO3[a]

atom	Cubic	$Tetr_{Ti}$	$Tetr_{Tio12}$	$Tetr_{exp}$
Ba	1.967 (0.6775)	1.956	1.935	1.917 (0.6577)
O1	−1.150 (−0.4264)	−1.138	−1.123	−1.121 (−0.3867)
O2	−1.150 (−0.4264)	−1.150	−1.159	−1.160 (−0.4916)
Ti	1.483 (0.5979)	1.483	1.506	1.526 (0.7086)

[a] For the atomic positions, see Figure 1. Values in parentheses are Hirshfeld charges.

tetragonal structure ($c = 4.0341$ Å, $a = 3.997$ Å). The calculated well depth (18.51 mev) is deeper by 5.61 meV than that one (12.9meV) at c/a=1, further indicating that the lattice strain strongly influences the potential energy surface, which is consistent with the LDA conclusion.[2−4] It is interesting to note that the contribution(∼6.5 meV) to well depth due to strain (at $c/a = 1.01$) calculated by FLPW(LDA)[3] is also close to our result (5.61meV). Above analyses and comparisons show that GGA and LDA predict the similar tendency of influence of lattice strain and lattice volume on potential surfaces.

3.3. Net Atomic Charges. In the above subsections we have discussed potential surfaces. Now we turn to electronic structures. Albeit the Mulliken population analysis[54] suffers from some shortcomings, it is still meaningful for some qualitative purposes in which chemists are interested.[55] We emphasize the net atomic charge, electronic populations, and bond orders to enforce the insight of chemical bonding for four structures of $BaTiO_3$.

Table 4 lists the Mulliken charges of four structures from BLYP calculations. Considering that the Mulliken charges are basis set dependent, we also present Hirshfeld charges[56] for the cubic and $Tetr_{exp}$ structures. Due to symmetry, all of the O atoms in the cubic structure are equivalent. In structures of $Tetr_{Ti}$, $Tetr_{TiO12}$, and $Tetr_{exp}$, O atoms are classified into two groups: the O atoms along the *Z*-axis (denoted as O1 in Figure 1) and the O atoms in XY plane (named O2). The calculated data in Table 4 exhibits the influence of atomic displacements (the Ti displacement and the coupled displacement of Ti, O1, and O2) and lattice strain on the charge distribution for those structures defined in Table 2.

In the ionic picture, Ba, Ti, and O atoms possess formal charges 2+, 4+, and 2−, respectively. In Table 4, the calculated Mulliken charges on Ba range from 1.967 (Cubic) to 1.917 ($Tetr_{exp}$). Meanwhile, charges of O and Ti atoms significantly deviate from their formal charges, implying that the Ti−O bond is partially ionic with some extent of covalency, which is in agreement with experiment.[57−59]

Let us examine Table 4 from left to right. The positive charges on Ba and the negative charges on O1 simultaneously decrease in proportion to the extent of atomic displacements and lattice strain during the phase transition. In consequence, Ba gains charges whereas O1 lose charges. Meanwhile, the atomic charges of O2 almost keep unchanged for different lattices, i.e., the O2 charge is insensitive to Ti displacement. However, from Cubic to $Tetr_{exp}$, the negative charges on O2 have been increased slightly. ref 12 pointed out that there was a charge transfer from Ba to O in tetragonal phase as the result of relative position shift and the small volume effect[The reported Ba charges are 1.39(Cubic) and 1.78(Tetragonal) respectively]. Namely Xu and co-workers think that from cubic to tetragonal phases Ba loses charges, which is different from ours. One possible reason for this discrepancy might be the different charge-partitioning schemes.

The positive charges on Ti also present an increasing trend in Table 4, indicating both lattice strain and coupled displacement of Ti and O atoms play the role of removing the electronic charge from Ti-sites. In one word, our results show that from cubic to tetragonal phase Ti and O1 lose charges whereas Ba and O2 gain charges.

TABLE 5: Electronic Populations in Atomic Orbitals

atom	AO	Cubic	$Tetr_{Ti}$	$Tetr_{Tio12}$	$Tetr_{exp}$
Ba	5s	1.865	1.864	1.868	1.869
Ba	6s	0.184	0.193	0.197	0.224
Ti	4s	0.136	0.124	0.116	0.085
Ti	$4p_x(4p_y)$	0.198	0.197	0.196	0.193
Ti	$4p_z$	0.198	0.190	0.180	0.169
Ti	$3d_{xy}$	0.486	0.492	0.490	0.479
Ti	$3d_{yz}(3d_{xz})$	0.488	0.470	0.468	0.455
Ti	$3d_{z^2}$	0.200	0.244	0.260	0.313
Ti	$3d_{x^2-y^2}$	0.200	0.207	0.207	0.216
O1	2s	1.829	1.833	1.834	1.841
O1	$2p_x(2p_y)$	1.796	1.778	1.772	1.755
O1	$2p_z$	1.722	1.739	1.747	1.759
O2	2s	1.829	1.832	1.827	1.833
O2	$2p_y$	1.722	1.707	1.708	1.700
O2	$2p_z$	1.796	1.803	1.827	1.816
O2	$2p_x$	1.796	1.801	1.802	1.805

It is evident from Table 4 that due to different charge partitioning schemes, the calculated Hirshfeld charges(absolute values) are much smaller than the corresponding Mulliken charges. However, the Hirshfeld charges also show that from Cubic to $Tetr_{exp}$, Ti and O1 lose charges whereas Ba and O2 gain charges, which are in qualitative agreement with Mulliken charge analyses.

3.4. Orbital Populations and Bond Orders. To shed light on the charge transfer, we have listed the electronic populations of atomic orbital (AO) in Table 5.

It is notable from the table that compared with the free atom configuration of Ba, each 5s AO loses about 0.13*e* and the electronic populations in 6s AOs range from 0.184*e* to 0.224*e*. Here one can see that most part of the charges obtained by 6s are offset by the charges lost from 5s. Both electronic populations of 5s and 6s AOs of Ba display an increase trend from cubic to tetragonal structures. However, the increment(0.040*e*) for 6s is much larger than that of 5s(0.004*e*). Obviously, the 6s AO is mainly the electron acceptor during the phase transition.

Similar comparison can be done for Ti. Comparing the electronic populations in each Ti AO for four structures, one can see that populations in almost all AOs diminish except for $3d_{x^2-y^2}$, and $3dz^2$ where the populations in the latter increase significantly. This may attribute to the formation of covalent bond between Ti and O atoms during the phase transition. The $3dz^2$ orbital is more bonded than $3d_{x^2-y^2}$ because of its symmetry adaptation in the tetragonal structures.

The electronic populations of $2p_z$ AO for O1 in Table 5 present an increase trend whereas the electronic populations on O1 decrease as a whole. This is in consistent with the trend of population in $3dz^2$ of Ti atom. Obviously, these two AOs adapt each other to form covalent bond of $3d_{z^2}-2p_z$ character between Ti and O1atoms along the tetragonal axis of the distorted lattice.

It can also be noted in Table 5 that the electronic populations in $2p_x$ of O2 increase in the same way while 2s and other 2p AOs look complicated.

Bond order relates to the covalent strength of a localized bond. The larger the bond order, the stronger the bond. Table 6 lists the calculated Mayer bond orders[60] between metal and oxygen atoms. The calculated Ti−O orders clearly show that Ti−O bonds have some extent of covalency. It is worth to point out that there is a debate on the Ba−O bond character as whether it is completely ionic[2−4] or has some covalency.[7−8] Our calculated Ba−O bond orders (ranging from 0.1156 to 0.1426)

TABLE 6: the Calculated Mayer Bond Orders[a]

bond	Cubic	$Tetr_{Ti}$	$Tetr_{Tio12}$	$Tetr_{exp}$
Ba−O1	0.1172	0.1156	0.1198	0.1339
Ba−O2	0.1172	0.1268	0.1268	0.1426
Ti−O1	0.5280	0.7610 (0.4640)	0.8230 (0.3418)	0.9958 (0.2930)
Ti−O2	0.5280	0.6111	0.6172	0.6708

[a] Values in the brackets are for the longer Ti−O1 bonds.

indicate that Ba−O bonds have certain extent of covalency, which is in agreement with the experiment[57] and band-band decomposition.[7−8]

The calculated bond orders indicate the enhancement of bonds in almost all cases when atomic displacements and lattice strain occur. Only Ba−O1 bond in $Tetr_{Ti}$ is slightly weakened by Ti displacement. Of course, in $Tetr_{Ti}$, $Tetr_{TiO12}$ and $Tetr_{exp}$ structures, one of the Ti−O1 is weakened due to the increase of Ti−O1 distance (see the values in brackets in Table 6). It is evident from Table 6 that bond strengths of Ba−O and Ti−O increase during the phase transition, which is consistent with the results that the kinetic energy increases and the potential energy decreases in pseudopotential calculations presented in 3.1. This provides an indirect support to the formation of new covalency due to distortion in the ferroelectric transition.[20] It is worth noting that the bond order of the shorter Ti−O1 increases the most (from 0.5280 to 0.9958), implying that Ti−O1 bond is the active part responsible for the ferroelectric phase transition of $BaTiO_3$.

4. Conclusion

DFT calculations result in a lattice constant of 3.99 Å and dielectric constant of 5.74 for the cubic $BaTiO_3$, in good agreement with the experiments. The calculated phonon frequencies also agree well with the experiment. The ferroelectric phase transition of $BaTiO_3$ is decisively induced by Ti displacement. Both lattice volume and lattice strain influence the potential surface. The larger the lattice volume and the ratio c/a the deeper the potential well. During the phase transition, Ba and O2 atoms gain charges whereas Ti and O1 lose charges. Our calculations show that Ba−O bond has some degree of covalency and the covalency between the shorter Ti−O1 is enhanced in proportional to the extent of distortion. Calculations also indicate that the covalent interaction between certain 3d AOs of Ti and 2p AOs of O plays an important role in stabilizing the ferroelectric tetragonal phase of $BaTiO_3$.

Acknowledgment. We are grateful to the referees for their valuable comments. One of the authors, Z.-X.C., thanks Dr. Chun-Gen Liu and Dr. Zi-Pin Bai for their kindly help.

References and Notes

(1) Lines, M. E.; Glass, A. M. *Principles and Applications of Ferroelectrics and Related Materials*; Clarendon Press: Oxford, 1977.
(2) Cohen R. E.; Krakauer, H. *Phys. Rev.*, **1990**, *B42*, 6416.
(3) Cohen, R. E. *Nature*, **1992**, *358*, 136.
(4) Cohen, R. E.; Krakauer, H. *Ferroelectrics*, **1992**, *136*, 65.
(5) Cohen, R. E.; Krakauer, H. *Ferroelectrics*, **1990**, *111*, 57.
(6) King-Smith, R. D.; Vanderbilt, D. *Ferroelectrics*, **1992**, *136*, 85.
(7) Ghosez, Ph.; Gonze, X.; Lambin, Ph.; Michenaud, J. P. *Phys. Rev.* **1995**, *B51*, 6765.
(8) Ghosez, Ph.; Michenaud, J. P.; Gonze, X. *Phys. Rev.* **1998**, *B58*, 6224.
(9) Zhong, W.; King-Smith, R. D.; Vanderbilt, D. *Phys. Rev. Lett.* **1994**, *72*, 3618.
(10) Ghosez, Ph.; Gonze, X.; Michenaud, J. P. *Ferroelectrics*, **1999**, *220*, 1.
(11) Xu, Y. N.; Ching, W. Y.; French, R. H. *Ferroelectrics*, **1990**, *111*, 23.
(12) Xu, Y. N.; Jiang, H.; Zhong, X. F.; Ching, W. Y. *Ferroelectrics* **1994**, *153*, 19.
(13) Miura, K.; Tanaka, M. *Jpn. J. Phys.* **1996**, *35*, 2719.
(14) Bagayoko, D.; Zhao, G. L.; Fan, J. D.; Wang, J. T. *J. Phys.: Condes. Matter* **1998**, *10*, 5645.
(15) Ghosez, Ph.; Gonze, X.; Michenaud, J. P. *Europhys. Lett.* **1996**, *33*, 713.
(16) Tinte, S.; Stachiotti, M. G.; Rodriguez, C. O.; Novikov, D. L.; Christensen, N. E. *Phys. Rev.* **1998**, *B58*, 11959.
(17) King-Smith, R. D.; Vanderbilt, D.*Phys. Rev.*, **1994**, *B49*, 5828.
(18) Zhong, W.; Vanderbilt, D. *Phys. Rev. Lett.* **1995**, *74*, 2587.
(19) Zhong, W.; Vanderbilt, D. *Phys. Rev. Lett.* **1994**, *73*, 1861.
(20) Bersuker, I. B. *Ferroelectrics* **1995**, *164*, 75.
(21) Weyrich, K. H. *Ferroelectrics* **1990**, *104*, 183.
(22) Weyrich, K. H.; Madenach, P. *Ferroelectrics*, **1990**, *111*, 9.
(23) Nelson, C. W. *M. I. T. Technol. Rep. Lab. Insulation Res.* **1963**, 179.
(24) Perdew, J. P.; Wang, Y. *Phys. Rev.* **1992**, *B46*, 6671.
(25) Singh, D. J. *Ferroelectrics* **1995**, *164*, 143.
(26) Ihm, J.; Zunger, A.; Cohen, M. L. *J. Phys. C* **1979**, *12*, 4409.
(27) Payne, M. C.; Teter, M. P.; Allan, D. C.; Arias, T. A.; Joannopoulos, J. D. *Rev. Mod. Phys.* **1992**, *64*, 1045.
(28) Yin, M. T.; Cohen, M. L. *Phys. Rev.* **1982**, *B26*, 5668.
(29) Hohenberg, P.; Kohn, W. *Phys. Rev.* **1964**, *136*, 864.
(30) Kohn, W.; Sham, L. J. *Phys. Rev.* **1965**, *140*, 1133.
(31) White, J. A.; Bird, D. M. *Phys. Rev.* **1994**, *B50*, 4954.
(32) Monkhorst, H. J.; Pack, J. D. *Phys. Rev.* **1976**, *B13*, 5188.
(33) Monkhorst, H. J.; Pack, J. D. *Phys. Rev.* **1977**, *B16*, 1748.
(34) Lin, J. S.; Qteish, A.; Payne, M. C.; Heine, V. *Phys. Rev.* **1993**, *B47*, 4174.
(35) Kleinman, L.; Bylander, D. M. *Phys. Rev. Lett.* **1982**, *48*, 1425.
(36) The experimental dielectric constant was obtained by extrapolating refractive index measurements at different wavelengths [Burns, G.; Dacol, F. H. *Solid State Commun.* **1982**, *42*, 9] to zero frequency, using a one-oscillator Sellmeyer equation.
(37) Milsui, T.; Nomura, S. *Numerical Data and Functional Relationships in Science and Technology*; Landolt-Bornstein III: New York, 1981; Vol. 16.
(38) Troullier, N.; Martins, J. L. *Phys. Rev.* **1991**, *B43*, 1993.
(39) Delley, B. *J. Chem. Phys.* **1990**, *92*, 508.
(40) Delley, B. *J. Chem. Phys.* **1991**, *94*, 7245.
(41) Ye, L.; Freeman, A. J.; Delley, B. *Phys. Rev.* **1989**, *B39*, 10144.
(42) Delley, B.; Wimmer, E. *J. Chem. Phys.* **1989**, *89*, 5177.
(43) Lemaire, G.; Hébant, P.; Picard, G. S. *J. Mol. Struct. (THEOCHEM)* **1997**, *419* (1−3), 1.
(44) Mryasov, O. N.; Freeman, A. J. *Mater. Sci. Eng.* **1999**, *260* (1−2), 80−93.
(45) Becke, A. D. *Phys. Rev.* **1988**, *A38*, 3098.
(46) Lee, C.; Yang, W.; Parr, R. G. *Phys. Rev.* **1988**, *B37*, 785.
(47) Kwei, G. H.; Lawson, A. C.; Billinge, S. J. L.; Cheong, S.-W. *J. Phys. Chem.* **1993**, *97*, 2368.
(48) Luspin, Y.; Servoin, J. L.; Gervais, F. *J. Phys. C*, **1980**, *13*, 3761.
(49) Rabe, K. M.; Waghmare, U. V. *Ferroelectrics* **1995**, *164*, 15.
(50) Ghosez, Ph.; Cockayne, E.; Waghare, U. V.; Rabe, K. M. *Phys. Rev.* **1999**, *B60*, 836.
(51) Slater, J. C. *Phys. Rev.* **1950**, *78*, 748.
(52) Decker, D. L.; Zhao, Y. X. *Phys. Rev.* **1989**, *B39*, 2432.
(53) Zhong, W. *Physics of Ferroelectric*; Scientific Press: Beijing, 1998.
(54) Mulliken, R. S. *J. Chem. Phys.* **1955**, *23*, 1833, 1841, 2338, 2343.
(55) Jensen, F. *Introduction to Computational Chemistry;* John Wiley & Sons: New York, 1999.
(56) Hirshfeld, F. L. *Theor. Chim. Acta*, **1944**, *44*, 129.
(57) Hudson, L. T.; Kurtz, R. L.; Robey, S. W.; Temple, D.; Stockbauer, R. L. *Phys. Rev.* **1993**, *B47*, 1174.
(58) Mattheiss, L. F. *Phys. Rev.* **1972**, *B6*, 4718.
(59) Pertosa, P.; Hollinger, G.; Michel-Calendini, F. M. *Phys. Rev.* **1978**, *B18*, 5177.
(60) Mayer, I. *Chem. Phys. Lett.* **1983**, *97*, 270.